Assessment of phosphorylation in Toxoplasma glideosome assembly and function

Jacot, Damien; Frenal, Karine; Marq, Jean-Baptiste; Sharma, Pushkar; Soldati-Favre, Dominique

How to cite

JACOT, Damien et al. Assessment of phosphorylation in Toxoplasma glideosome assembly and function. In: Cellular microbiology, 2014, vol. 16, n° 10, p. 1518–1532. doi: 10.1111/cmi.12307

This publication URL: https://archive-ouverte.unige.ch/unige:39626
Publication DOI: 10.1111/cmi.12307

Cellular Microbiology (2014) doi:10.1111/cmi.12307

Assessment of phosphorylation in *Toxoplasma* glideosome assembly and function

Damien Jacot,[1] Karine Frénal,[1] Jean-Baptiste Marq,[1] Pushkar Sharma[2] and Dominique Soldati-Favre[1]*

[1]*Department of Microbiology & Molecular Medicine, CMU/University of Geneva, Rue Michel-Servet 1, CH-1211 Geneva 4, Switzerland.*

[2]*Eukaryotic Gene Expression Laboratory, National Institute of Immunology, New Delhi 110067, India.*

Summary

Members of the phylum Apicomplexa possess a highly conserved molecular motor complex anchored in the parasite pellicle and associated with gliding motility, invasion and egress from infected cells. This machinery, called the glideosome, is structured around the acylated gliding-associated protein GAP45 that recruits the motor complex composed of myosin A and two associated myosin light chains (TgMLC1 and TgELC1). This motor is presumably firmly anchored to the inner membrane complex underneath the plasma membrane via an interaction with two integral membrane proteins, GAP50 and GAP40. To determine if the previously mapped phosphorylation sites on TgGAP45 and TgMLC1 have a direct significance for glideosome assembly and function, a series of phospho-mimetic and phospho-null mutants were generated. Neither the overexpression nor the allelic replacement of TgMLC1 with phospho-mutants impacted on glideosome assembly and parasite motility. TgGAP45 phosphorylation mutants were functionally investigated using a complementation strategy in a TgGAP45 inducible knockout background. The loss of interaction with TgGAP50 by one previously reported GAP45-mutant appeared to depend only on the presence of a remaining competing wild type copy of TgGAP45. Accordingly, this mutant displayed no phenotype in complementation experiments. Unexpectedly, GAP45 lacking the region encompassing the cluster of twelve phosphorylation sites did not impact on its dual function in motor recruitment and pellicle integrity. Despite the extensive phosphorylation of TgMLC1 and TgGAP45, this post-translational modification does not appear to be critical for the assembly and function of the glideosome.

Received 21 November, 2013; accepted 16 April, 2014. *For correspondence. E-mail dominique.soldati-favre@unige.ch; Tel. (+41) 22 379 5672; Fax (+41) 22 379 5702.

Introduction

Members of the Apicomplexa are responsible for a wide range of diseases in both humans and animals. This large group of obligate intracellular parasites includes *Toxoplasma gondii* which affects humans and warm-blooded animals and causes toxoplasmosis (Montoya and Liesenfeld, 2004), and *Plasmodium* species, the causative agents of malaria that lead to hundreds of thousands of deaths per year (Murray *et al*., 2012). Most invading stages of the Apicomplexans are capable of migrating across biological barriers and actively penetrate and egress from host cells by a mechanism that relies on substrate-dependent motion. This gliding motility requires actin polymerization (Dobrowolski and Sibley, 1996; Wetzel *et al*., 2003) and is powered by a large molecular machine called the glideosome. This complex is highly and exclusively conserved across the phylum and positioned at the parasite pellicle, within the narrow space that separates the plasma membrane (PM) from the inner membrane complex (IMC) composed of flattened cisternae (Morrissette and Sibley, 2002).

In *T. gondii*, the glideosome has been extensively characterized and is composed of a myosin heavy chain (TgMyoA) (Herm-Gotz *et al*., 2002; Meissner *et al*., 2002), two associated light chains TgMLC1 (myosin light chain 1) (Herm-Gotz *et al*., 2002) and TgELC1 (essential light chain 1) (Nebl *et al*., 2011), the peripheral membrane protein TgGAP45 (gliding associated protein 45) (Gaskins *et al*., 2004) and two integral IMC proteins TgGAP50 and TgGAP40 (Gaskins *et al*., 2004; Frenal *et al*., 2010). The motor complex composed of TgMyoA/TgMLC1/TgELC1 is recruited via the C-terminal part of TgGAP45 at the pellicle where it interacts with TgGAP40 and/or TgGAP50 (Gaskins *et al*., 2004; Frenal *et al*., 2010). In addition, TgGAP45 is anchored to the PM via N-terminal acylations and constitutes a fluid bridge between the two membranes of the pellicle to maintain their cohesion (Rees-Channer *et al*., 2006; Frenal *et al*., 2010). During

motility and invasion, microneme contents are discharged apically in response to a rise in intracellular calcium and the adhesins released onto the parasite surface form complexes with the extracellular matrix or the host cell receptors (Carruthers and Boothroyd, 2007). Presumably, the glideosome generates a forward motion by translocation of the adhesin-receptor complexes to the posterior pole of the parasite (Opitz and Soldati, 2002; Keeley and Soldati, 2004). TgGAP45 and TgMyoA have been reported to be central for all three experimentally assessable functions of the glideosome: gliding, invasion and egress (Meissner *et al*., 2002; Frenal *et al*., 2010; Andenmatten *et al*., 2013).

The glideosome is predicted to be tightly controlled, both temporally and spatially and several studies point towards an important role for phosphorylation in its assembly and, or function. Phosphorylation on residues S163 and S167 of TgGAP45 was reported to play a role in the final assembly of the glideosome, as transient expression of a phosphomimetic mutant failed to associate with TgGAP50. Specifically, this indicated that dephosphorylation is required for the final anchoring step at the IMC and this loss of interaction was speculated to be critical (Gilk *et al*., 2009). *P. falciparum* late schizont stage parasites treated with a broad-range serine/threonine kinase inhibitor (staurosporine) showed a significant reduction in phosphorylated forms of PfGAP45 resulting in a important decrease in interaction with the actomyosin motor (Jones *et al*., 2009). Furthermore, PfGAP45 was reported to interact with and to be phosphorylated *in vitro* by the protein kinase B (PfPKB) (Vaid *et al*., 2008; Thomas *et al*., 2012). Additionally, *in vitro* phosphorylation assays also identified PfCDPK1 (calcium-dependent protein kinase 1), which is localized to the PM of *P. falciparum* merozoites and is the potential kinase phosphorylating PfGAP45 and PfMTIP (MyoA tail-interacting protein), the homologue of TgMLC1 in the malaria parasite (Green *et al*., 2008; Kato *et al*., 2008; Winter *et al*., 2009; Tewari *et al*., 2010; Azevedo *et al*., 2013). Phosphorylation of PfGAP45 at S103 and S149, two of the PfCDPK1 target sites, was also observed in the parasite (Ridzuan *et al*., 2012; Thomas *et al*., 2012). Finally, PfPKA also phosphorylates PfGAP45 and PfMyoA *in vitro* (Lasonder *et al*., 2012).

Microneme secretion is triggered by changes in intracellular calcium levels (Carruthers and Sibley, 1999; Lovett and Sibley, 2003; Billker *et al*., 2009; Lourido *et al*., 2012). Invasion and egress from infected cells are tightly connected to microneme secretion and demonstrated to depend on the action of TgCDPK1 and TgCDPK3 in *T. gondii* (Lourido *et al*., 2010; 2012; Garrison *et al*., 2012; McCoy *et al*., 2012). Using comparative phosphoproteome analyses in *T. gondii*, several residues in TgGAP45, TgMLC1 and TgMyoA, for which phosphorylation was selectively increased upon calcium stimulation, were identified (Nebl *et al*., 2011). Finally, global phosphoproteome analyses of *T. gondii* and *P. falciparum* (Solyakov *et al*., 2011; Tyler *et al*., 2011; Lasonder *et al*., 2012; Pease *et al*., 2013) revealed extensive phosphorylation of various components of the glideosome with up to 35 and 25 sites respectively (Jacot and Soldati-Favre, 2012). While the identity of phosphorylation sites on these proteins is clear, the functional implications of phosphorylation remain unknown.

Here we functionally assessed the importance of recently mapped phosphorylation sites on TgMLC1 and TgGAP45 via the generation of parasite lines expressing phosphorylation mutants. Results indicated that the phosphorylation of most sites on TgGAP45 and TgMLC1 is dispensable for glideosome assembly and parasite motility. The GAP45-S163/7E mutant previously reported to lose interaction with TgGAP50 was confirmed only in the presence of the wild type (wt) inducible copy of TgGAP45, which likely competes for association with GAP50. In contrast, GAP45-S163/7E interaction with GAP50 was restored in the absence of GAP45 and allelic replacement of *TgGAP45* with this mutant had no impact on parasite fitness.

Results

Phosphorylation of TgMLC1

To investigate the impact of TgMLC1 phosphorylation on the glideosome (Figs 1A and S1A), a first strategy was based on overexpression of TgMLC1 mutated second copies. A destabilization domain (DD) and a Myc tag were fused to the N-terminus of TgMLC1 for rapid and tight control of TgMLC1 expression upon addition of shield (Shld-1) (Herm-Gotz *et al*., 2007). Residues S55, S98 and T132 have previously been reported to be phosphorylated with the latter two showing a significant increase in phosphorylation when parasites were stimulated with calcium ionophore (Nebl *et al*., 2011). We first generated mutants at each individual site where the amino acid residue was mutated to either an alanine (phospho-null) or to a glutamic acid (phospho-mimetic). No phenotype was observed by plaque assay and no alteration of the glideosome composition was monitored by co-immunoprecipitation (co-IP) upon conditional stabilization of the mutants (data not shown). We then generated triple mutants where phosphorylation sites S55, S98 and T132 were mutated to alanine (DDMycMLC1-AAA) or to glutamic acid (DDMycMLC1-EEE). The construct DDMycMLC1-wt was included as a control for comparison. Expression of all the mutants was undetectable unless Shld-1 was added to the culture. Upon stabilization of the DDMycMLC1 second copies, the level of endogenous MLC1 was dramatically reduced (Fig. 1B). It was

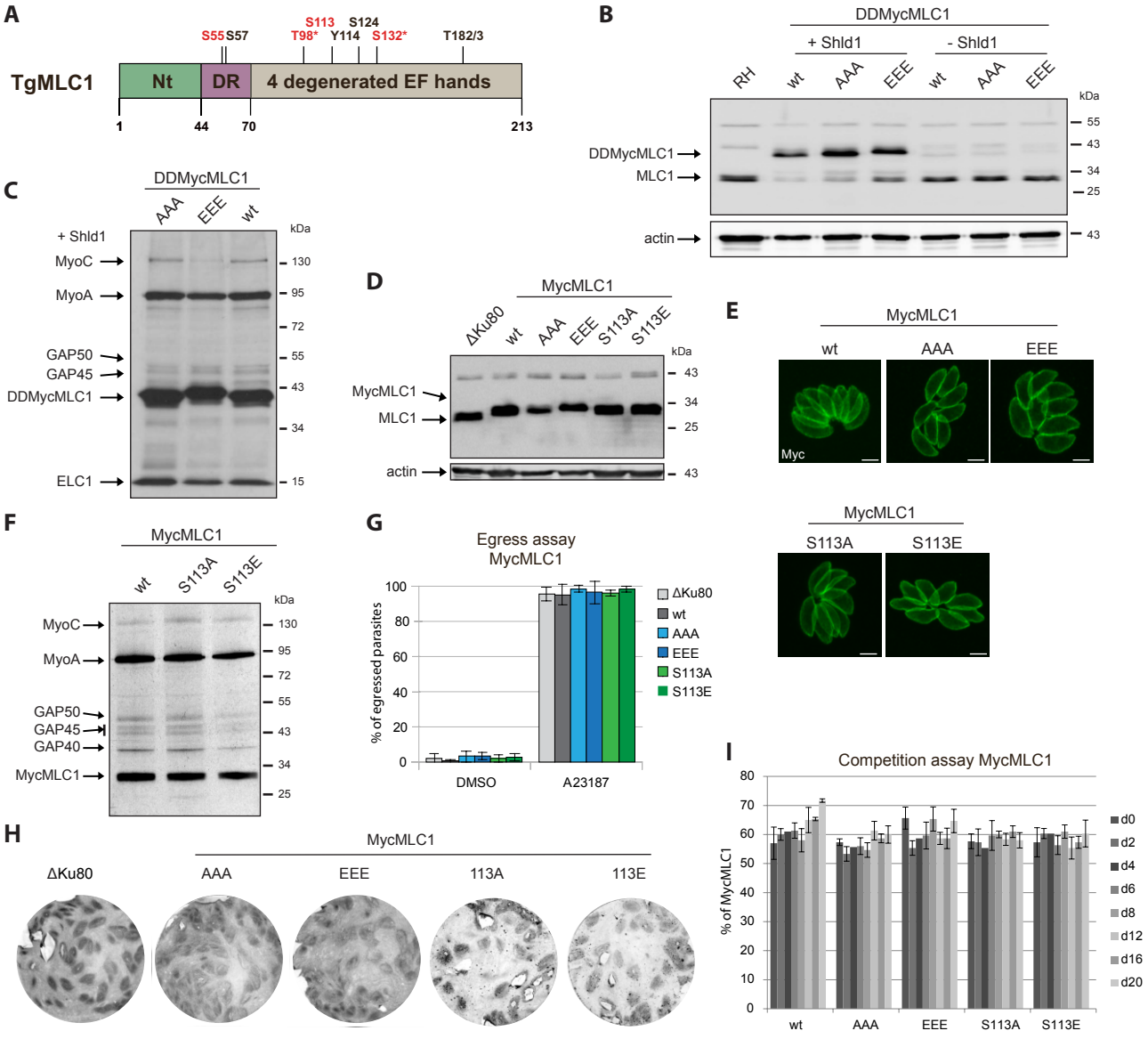

Fig. 1. Phosphorylation of TgMLC1.
A. Schematic representation of TgMLC1 phosphorylation sites (Treeck *et al.*, 2011). The sites investigated in this study are highlighted in red and the calcium-dependent phosphorylation sites are indicated by a star. Nt, N-terminus; DR, disordered region (Nebl *et al.*, 2011).
B. Western blot analyses using anti-MLC1 antibodies of DDMycMLC1 and RH strains treated for 24 h ± Shld-1. Expression of DDMycMLC1 (38 kDa) was only observed in the presence of Shld-1 and resulted in destabilization of the endogenous TgMLC1 (24 kDa). Detection of *T. gondii* actin (TgACT1) was used as a loading control.
C. Metabolic labelling with ^{35}S-methionine/cysteine followed by co-IP using anti-Myc antibodies revealed no alteration in the glideosome composition.
D. Western blots performed with anti-MLC1 antibodies on the different strains of TgMLC1 generated by knock-in. A slight molecular-weight shift was observed compared with the wild type (ΔKu80) due to the presence of the Myc tag. TgACT1 detection is included as a loading control.
E. Immunofluorescence analyses (anti-Myc) revealed no alteration of the localization at the pellicle. Scale bar 2 μm.
F. Metabolic labelling with ^{35}S-methionine/cysteine followed by co-IP using anti-Myc antibodies showed no alteration of the glideosome composition. No reduction of co-IP MyoA was observed for MycMLC1-S113E.
G–I. No phenotype was observed in calcium ionophore-induced egress, plaque assay, or competition experiments for all the phosphorylation sites investigated by knock-in compared with the parental strain (ΔKu80).

previously reported that the level of MLCs are regulated by their capacity to associate with their corresponding myosin heavy chain (Polonais *et al*., 2011). In consequence, the drop in the endogenous level of TgMLC1 suggested that the mutated copies were assembled with TgMyoA. All the mutants localized to the pellicle and displayed no defect by plaque assay when compared with DDMycMLC1-wt (Fig. S1B and C). The composition of the glideosome in the different parasite lines was assessed by co-IP with anti-Myc antibodies following metabolic labelling with ^{35}S-methionine and cysteine (Fig. 1C). The band migrating at 130 kDa corresponds to myosin C (TgMyoC), which associates with TgMLC1 and composes the MyoC-glideosome (K. Frénal, J.B. Marq, V. Polonais and D. Soldati-Favre, unpublished). Only the mutant DDMycMLC1-EEE displayed a reduction in its ability to bind TgMyoC while the other mutants were not affected when compared with DDMycMLC1-wt.

Since residual expression of endogenous MLC1 was still detectable in transgenic parasites upon stabilization of MLC1 mutants, we opted for an allelic replacement approach to obtain a definitive answer. The composition of the *TgMLC1* locus includes an unusually long 5′ UTR that was used to introduce mutated forms of *TgMLC1* downstream of the promoter by single homologous recombination (knock-in). This resulted in displacement of the endogenous open reading frame (Fig. S1D). The same AAA, EEE and wt mutants tagged in their N-terminus with a Myc tag were generated (MycMLC1-AAA, -EEE, -wt). In addition, we have generated the single mutants MycMLC1-S113A and MycMLC1-S113E, based on the report that the interaction of PfMTIP and PfMyoA might be specifically modulated by phosphorylation at residues S107 and/or S108 of PfMTIP. Specifically, phosphomimetic mutants at both residues were reported *in vitro* to weaken the tight clamp around PfMyoA (Douse *et al*., 2012). These two residues align with residues S113 and Y114 of TgMLC1 (Fig. S1A) that have also been identified *in vivo* to be phosphorylated (Tyler *et al*., 2011). As a negative control, we replaced MycMLC1-wt in the transfection plasmid with DsRed and despite several transfections; we failed to obtain any positive pools proving that the *TgMLC1* locus cannot be disrupted unless an additional copy of *TgMLC1* is integrated.

All MycMLC1 constructs were integrated accurately at the *TgMLC1* genomic locus as demonstrated by genomic PCR analysis (Fig. S1E). Western blot analyses using anti-MLC1 antibodies confirmed the gene displacement diagnosed by the slight shift in molecular weight accounted for by the Myc tag compared with endogenous TgMLC1 (Fig. 1D). The MycMLC1 mutants showed the same localization as MycMLC1-wt (Fig. 1E). In addition, the single mutations S113A and S113E did not affect the association of TgMLC1 with TgMyoA or with the rest of the complex (Fig. 1F). Transgenic parasites displayed no impairment in calcium ionophore-induced egress (Fig. 1G), formed plaques of similar sizes compared with the parental strain (Fig. 1H) and showed no defect in intracellular growth (Fig. S1F). To assess the contribution of more subtle changes that could not be detected in the previous assays, we performed competition experiments with all MycMLC1 strains. The different transgenic lines were co-cultured with a parental strain over an extended period of time but significant alteration in the ratio of parental versus transgenic strains was not observed (Fig. 1I).

To determine if mutation of the three phosphorylation sites S55, S98 and T132 resulted in compensatory phosphorylation elsewhere in the molecule, MycMLC1-AAA and MycMLC1 were co-immunoprecipitated using anti-Myc antibodies and analysed by mass spectrometry after phosphopeptides enrichment. Two of the nine previously reported phosphorylation sites in MLC1 were identified in the MycMLC1-wt sample (T98 and S124) as well as two additional ones at residues S92 and S97 (Fig. S3A and B). In MycMLC1-AAA analyses, the two sites S97 and S124 were also found phosphorylated as well the serine S57 close to the mutated S55 (Fig. S3C).

Taken together, these results indicate that the phosphorylation sites investigated here do not critically impact TgMLC1 function and its assembly within the glideosome although cryptic phosphorylation on neighbouring site might have a functional compensatory effect.

Phosphorylation of TgGAP45

The importance of phosphorylation for TgGAP45 function was investigated by complementation of the inducible knockout strain of TgGAP45 (ΔGAP45e/MycGAP45i) (Frenal *et al*., 2010) with phosphorylation mutants. These mutants were Ty-tagged between the conserved N-terminus and the coiled-coil region to distinguish them from the inducible copy MycGAP45i (Figs 2A and S2, TyGAP45c). Stable clones of four double and four single mutants were generated with either an alanine or a glutamic acid substitution (TyGAP45c-S163/7A, S163/7E, S184/5A, S184/5E, T189A, T189E, S239A and S239E). All residues were reported to be phosphorylated *in vivo* (Tyler *et al*., 2011) and residues S184/5 and T189 showed increased phosphorylation upon stimulation of calcium signalling (Nebl *et al*., 2011). Additionally, a strain complemented with a wild type version of TgGAP45 was generated (TyGAP45c-wt). The complementing copies were expressed at comparable levels in ΔGAP45e/MycGAP45i and the tight regulation of MycGAP45i by ATc was preserved (Fig. 2B). The mutants and the wt showed proper localization to the pellicle either in the presence or absence of ATc (Fig. 2C). No phenotype was observed by plaque assay upon addition of ATc for the complemented

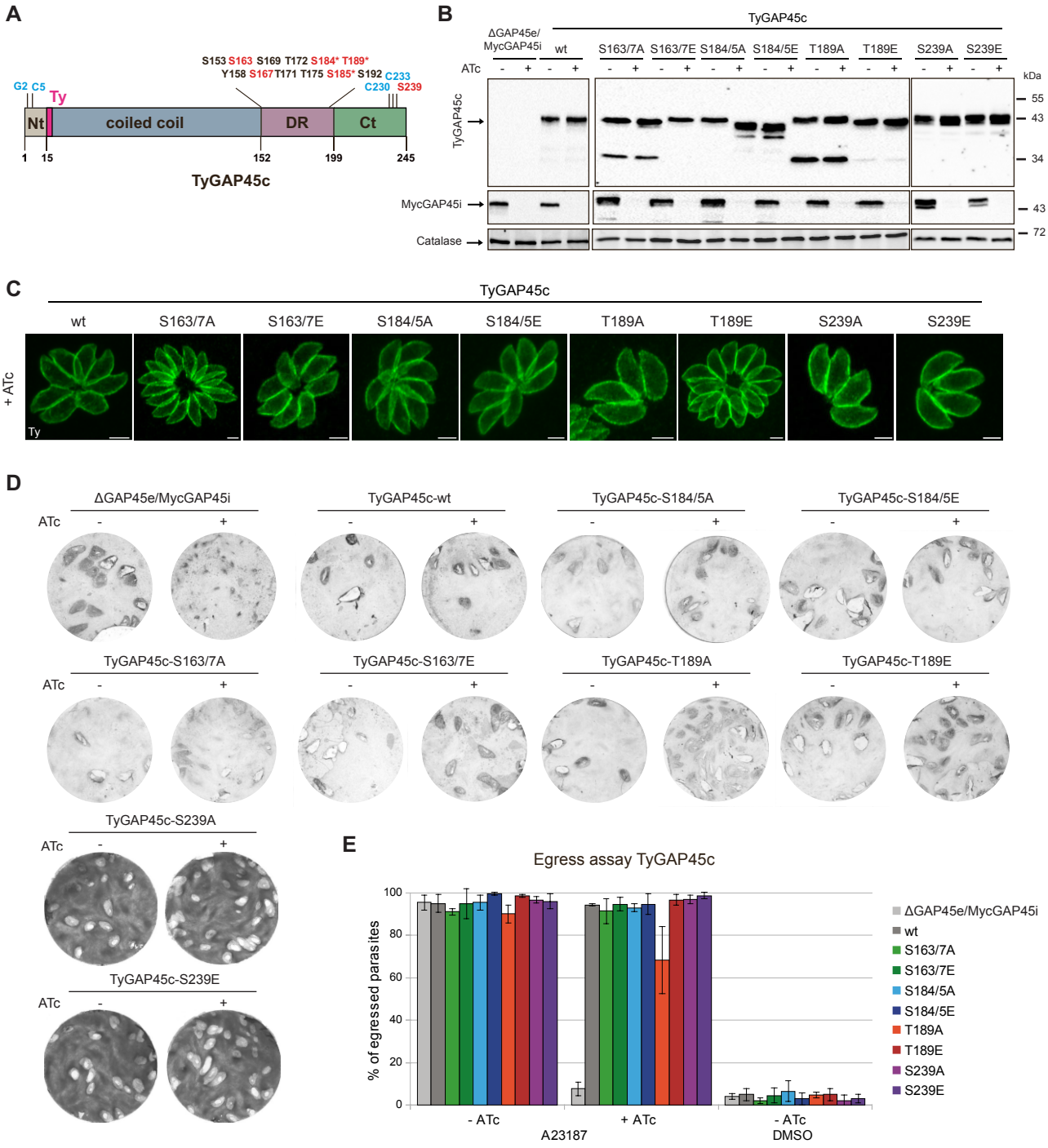

Fig. 2. Complementation of the inducible knockout strain of TgGAP45 with phosphorylation mutants.
A. Schematic representation of TgGAP45 post-translational modifications (Frenal *et al.*, 2010; Nebl *et al.*, 2011; Treeck *et al.*, 2011). The phosphorylation sites investigated in this study are highlighted in red, sites not investigated are highlighted in black and the stars indicate the calcium-dependent phosphorylation sites. The putative myristoylation (G) and palmitoylation (C) sites are highlighted in blue, Nt, conserved N-terminus; Ct, conserved C-terminus; DR, disordered region. The Ty tag was not included in the amino acid numbering.
B. All complemented TyGAP45 strains are expressed at similar levels by western blot analyses using anti-Ty antibodies. Regulation of MycGAP45i was assessed with anti-Myc antibodies after 48 h ± ATc. Detection of *T. gondii* catalase was used as a loading control.
C. Immunofluorescence analyses (anti-Ty) revealed no alteration in the localization at the pellicle. Scale bar 2 μm.
D. The complemented strains formed plaques of similar sizes ± ATc. In contrast, no plaque was formed in ΔGAP45e/MycGAP45i in the presence of ATc.
E. Only mutant TyGAP45c-T189A showed a 30% reduction in calcium ionophore-induced egress after 48 h of ATc treatment. Parasites lacking TgGAP45 (ΔGAP45e/MycGAP45i + ATc) were severely affected in egress.

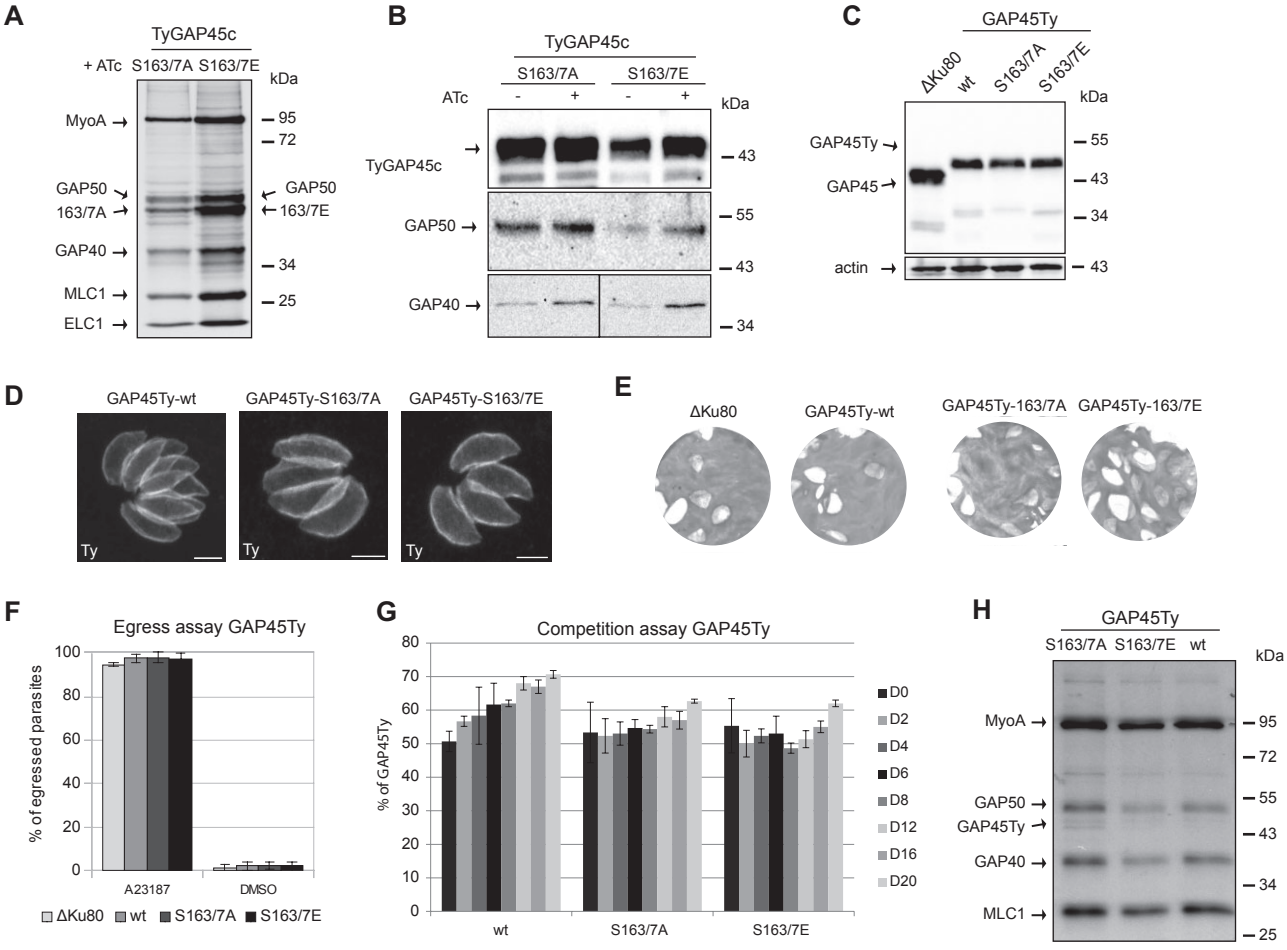

Fig. 3. In-depth analysis of residues S163/7.
A. Co-IPs using anti-Ty antibodies with ^{35}S-methionine/cysteine metabolically labelled TyGAP45c-S163/7E and -S163/7A revealed no alteration of the glideosome composition in the presence of ATc.
B. Same co-IPs as in (A) but parasites were pre-treated ± ATc for 48 h. In the absence of ATc, TyGAP45c-S163/7E was partially impaired in its ability to interact with the IMC resident proteins TgGAP40 and TgGAP50.
C. Western blot analyses of the GAP45Ty-wt, -S163/7A and -S163/7E revealing a slight molecular weight shift compared with the endogenous TgGAP45 (ΔKu80) due to the presence of the Ty tag. Anti-GAP45 antibodies were used for probing. Detection of TgACT1 was used as a loading control.
D. Immunofluorescence analyses (anti-Ty) revealed no alteration of the localization at the pellicle. Scale bar 2 μm.
E–G. All GAP45Ty parasites formed plaques of similar sizes to ΔKu80, were not affected in egress from infected cells and displayed no significant phenotypes in competition experiments.
H. Co-IPs using anti-GAP45 antibodies with ^{35}S-methionine/cysteine metabolically labelled TyGAP45c-wt, -S163/7E and -S163/7A revealed no alteration in glideosome composition.

strains while ΔGAP45e/MycGAP45i formed no visible plaques (Fig. 2D). Calcium ionophore-induced egress assays revealed that the mutant TyGAP45c-T189A displayed only a slight reduction in egress from infected host cells in the presence of ATc while the control ΔGAP45e/MycGAP45i was severely impaired (Fig. 2E).

Unexpectedly, the mutant TyGAP45c-S163/7E previously reported to lose interaction with TgGAP50 (Gilk *et al.*, 2009) was readily generated and displayed no phenotype in both RH (data not shown) and in the ΔGAP45e/MycGAP45i background. Co-IPs using anti-Ty antibodies in the presence of ATc resulted in no alteration of glideosome composition, hence contrasting with the previously reported findings (Fig. 3A). In order to resolve this discrepancy, we repeated the experiment in the presence or absence of ATc. In the absence of ATc, TyGAP45c-S163/7E displayed a partial loss of interaction with TgGAP50 and TgGAP40. This association was re-established in the presence of ATc (Fig. 3B). This suggested that the MycGAP45i wt copy efficiently competes for binding with GAP50 and likely explains the result obtained by Gilk *et al.* (2009), where only transient transfections in wt parasites were performed. Of relevance, the level of TgGAP50 was also found to slightly

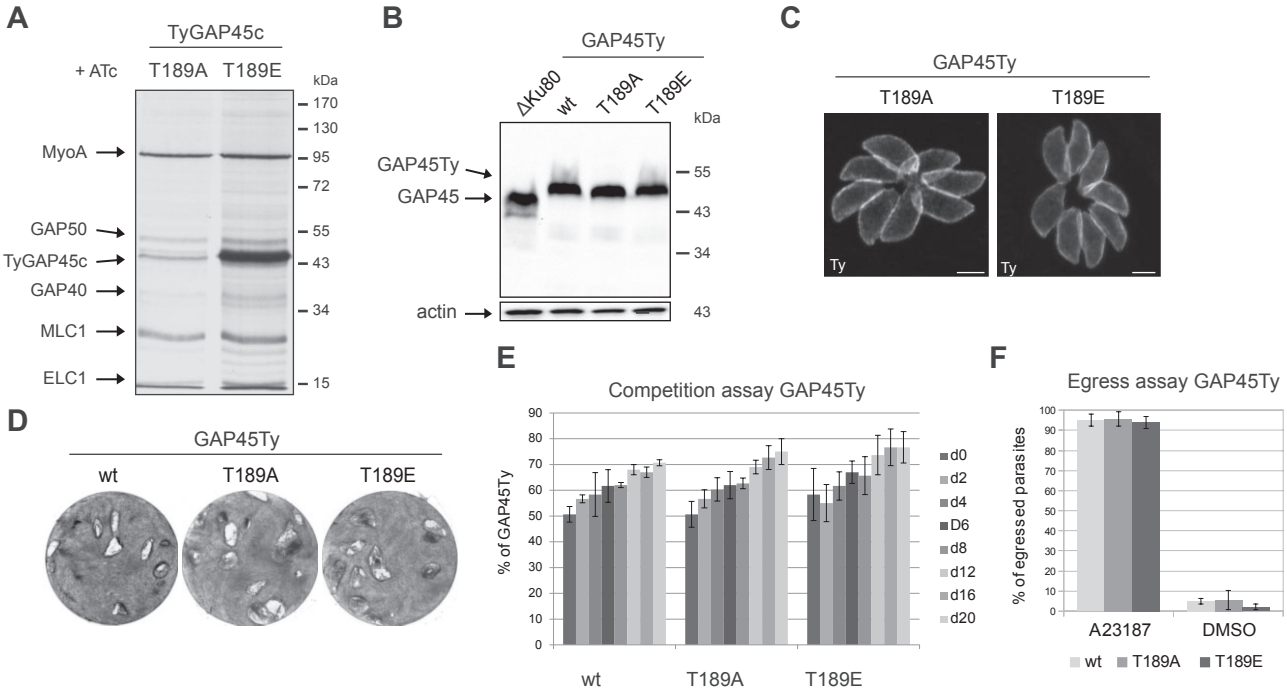

Fig. 4. In-depth analysis of residue S189.
A. Metabolic labelling with ^{35}S-methionine/cysteine followed by co-IP using anti-Ty antibodies revealed no alteration in glideosome composition for the mutants TyGAP45c-T189A and -T189E.
B. Western blot analyses of the GAP45Ty knock-in strains showed a slight molecular weight shift compared with the endogenous TgGAP45 (ΔKu80) due to the presence of the Ty tag. Anti-GAP45 antibodies were used for probing. Detection of TgACT1 was used as loading control.
C. All GAP45Ty properly localized to the pellicle by immunofluorescence using anti-Ty antibodies. Scale bar 2 μm.
D and E. All GAP45Ty parasites formed plaques similar in size to ΔKu80 and showed similar kinetics in competition experiments.
F. In contrast to the complementation experiments, GAP45Ty-T189A showed no defect in calcium ionophore-induced egress.

fluctuate in the mutant S163/7A cultivated in the presence or absence of ATc. Accordingly, the level of co-immunoprecipitated TgGAP40 mirrored the level of TgGAP50 (Fig. 3B). To further consolidate this observation, we substituted *TgGAP45* by single homologous recombination (knock-in) at the endogenous locus with either TyGAP45c-wt or the two corresponding phospho-null or phospho-mimetic-mutants, Ty-tagged just upstream of the predicted disorganized region (GAP45Ty-wt, -S163/7A, -S163/7E). This caused a small shift in the apparent molecular weight observed by western blot using anti-GAP45 antibodies (Fig. 3C). Both GAP45Ty mutants and TyGAP45c-wt localized to the pellicle (Fig. 3D) and no phenotype was observed by plaque assay or by calcium-ionophore induced egress (Fig. 3E and F). In addition, both phospho-mutants were not overgrown by the parental strain in competition experiments although TyGAP45c-wt parasites appeared to grow very modestly better (Fig. 3G). Concordantly, the composition of the glideosome and specifically the association with TgGAP50 and TgGAP40 were not affected in co-IPs using anti-GAP45 antibodies (Fig. 3H).

In the calcium ionophore-induced egress assays only the TyGAP45c-T189A expressing mutant displayed a slight reduction in egress from infected host cells in the presence of ATc (Fig. 2E). The assembly of the glideosome was further examined for this mutant and it was found that all the components were assembled properly (Fig. 4A). Of relevance, the majority of TyGAP45c-T189A expressing clones showed lower levels of expression compared with TyGAP45c-T189E that resulted in a strong phenotype both by plaque assay and induced egress. We did however succeed in obtaining clones such as the one reported here, which exhibited a level of expression comparable to the other mutants. To complement the characterization of these mutants, we compared the half-lives of TyGAP45c-T189A and wt GAP45 by performing pulse-chase experiments and found no difference in protein turnover suggesting that the absence of phosphorylation did not significantly affect the stability of the protein (data not shown). To rule out the possibility that the slight phenotype observed in the complementation experiment using the mutant TyGAP45c-T189A was due to an insufficient protein level, we substituted the *TgGAP45* locus with the two mutants as previously described (GAP45Ty-T189A, -T189E). Western blot analyses using anti-GAP45 antibodies revealed the expected small shift in molecular weight

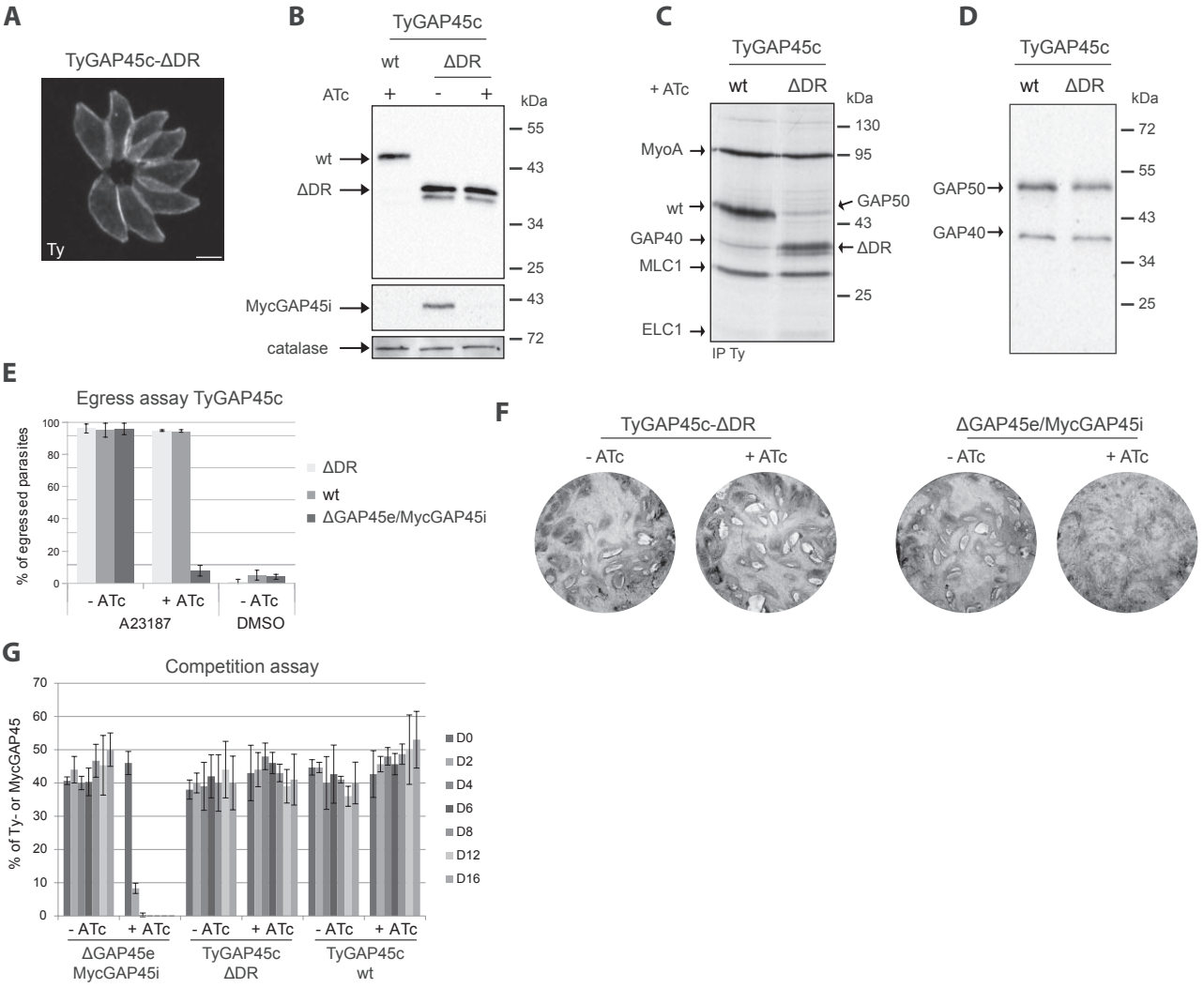

Fig. 5. TgGAP45 disordered region deletion mutant.
A. TyGAP45c-ΔDR is correctly localized to the pellicle. Scale bar 2 μm.
B. TyGAP45c-ΔDR is found with the expected molecular weight shift compared with TyGAP45c-wt by western blot analyses using anti-Ty antibodies. Regulation of MycGAP45i was assessed with anti-Myc antibodies after 48 h in the presence of ATc. Detection of *T. gondii* catalase was used as a loading control.
C. No alteration of the glideosome composition was observed for TyGAP45c-ΔDR by ^{35}S-methionine/cysteine metabolic labelling followed by co-IP using anti-Ty antibodies.
D. Western blot analyses of the same samples using anti-GAP40 and anti-GAP50 antibodies revealed that both proteins co-immunoprecipitate equally in both TyGAP45c-wt and TyGAP45c-ΔDR.
E–G. In contrast to ΔGAP45e/MycGAP45i, TyGAP45c-ΔDR parasites are not affected in calcium ionophore-induced egress (E), plaque formation (F) or competition experiments (G) ± ATc.

compared with the parental strain (ΔKu80) (Fig. 4B). Genomic PCR analyses were performed and sequencing of the products confirmed the presence of the mutation at the modified TgGAP45 locus (data not shown). These GAP45Ty mutants displayed a correct localization to the pellicle (Fig. 4C) and no phenotype was observed by plaque and competition assays when to compared with GAP45Ty-wt (Fig. 4D and E). In contrast to the complementation experiments using TyGAP45c-T189A in ΔGAP45e/MycGAP45i, no impairment in egress was observed with the GAP45Ty-T189A strain generated by knock-in (Fig. 4F).

Twelve of the 13 phosphorylation sites mapped on TgGAP45 are clustered in the predicted disordered region (DR) (Nebl *et al*., 2011) (Fig. 2A). Since individual point mutations had no impact on the assembly and function of the glideosome, we complemented ΔGAP45e/MycGAP45i with a TgGAP45 deletion mutant lacking this entire disordered region (TyGAP45c-ΔDR; Fig. S2). TyGAP45c-ΔDR localized to the pellicle (Fig. 5A), was

expressed at a similar level compared with the TyGAP45c-wt and migrated at the predicted weight on SDS-PAGE. Importantly, MycGAP45i remained tightly regulated by ATc in this mutant (Fig. 5B). The assembly of the glideosome was not affected in TyGAP45c-ΔDR based on co-IP experiments on metabolically labelled parasites (Fig. 5C). The presences of TgGAP50 and TgGAP40 in the co-IP were further confirmed by western blot analyses on the same samples using the corresponding antibodies (Fig. 5D). Phenotypic investigation of this mutant in the presence of ATc revealed no defect in plaque formation or calcium ionophore-induced egress, while the control ΔGAP45e/MycGAP45i failed to form visible plaques and to egress in the presence of ATc as previously reported (Fig. 5E and F). No significant change was observed in competition experiments for TyGAP45c-ΔDR ± ATc while ΔGAP45e/MycGAP45i + ATc was over-grown by the parental strain at day 2 (Fig. 5G). Importantly, MycGAP45i was still regulated by ATc at day 16 in both TyGAP45c-ΔDR and control TyGAP45c-wt parasites. To rule out the possibility that deletion of the DR results in compensatory phosphorylation elsewhere in the molecule, TyGAP45c-ΔDR and TyGAP45c-wt were co-immunoprecipitated using anti-Ty antibodies and analysed by mass spectrometry. Seven of the eleven previously reported phosphorylation sites in the DR as well as an additional phosphorylation site at residue T199 were identified in the TyGAP45c-wt samples (Fig. S4A and B). TyGAP45c-ΔDR analyses revealed no additional phosphorylation in the vicinity of the DR but one cryptic phosphorylation was found in the Ty tag (Fig. S4B). Importantly, in both analyses residue S239 was found to be phosphorylated.

Taken together, these data establish that phosphorylation of TgGAP45 is dispensable for glideosome assembly and function.

Discussion

Since the components of the glideosome are abundantly phosphorylated both in *T. gondii* and *P. falciparum* (Nebl *et al*., 2011; Solyakov *et al*., 2011; Tyler *et al*., 2011; Lasonder *et al*., 2012; Pease *et al*., 2013), it was anticipated that this post-translational modification could regulate the assembly and impact on the activity of the motor complex. Using two independent approaches that involved either overexpression or allelic replacement with phosphorylation mutants, we demonstrated that several of the reported sites on TgMLC1 were non-critical for the glideosome functions. In addition to TgMyoA, TgMLC1 also associates with TgMyoC (K. Frénal, J.B. Marq, V. Polonais and D. Soldati-Favre, unpublished). This myosin localizes to the anterior and posterior polar rings and overexpression of the alternatively spliced variant TgMyoB was associated with pellicle integrity during replication (Delbac *et al*., 2001). In consequence, we assessed the intracellular growth but recorded no defect with the MLC1-EEE mutant that exhibited a loss of interaction with TgMyoC. Importantly, competition experiments that are best suited to score minor loss of fitness also failed to reveal any defect.

Out of the four sites that were not investigated, two (S57 and S124) are poorly conserved in the TgMLC1 sequence across the phylum, and the other two (T182 and/or T183) are surrounded by negatively charged residues conserved in other Apicomplexa (Fig. S1A). In the case of PfMTIP, the only residues found to be phosphorylated *in vivo* are the S107 and/or S108. *In vitro* studies suggested that these phosphorylation sites might modulate the interaction between PfMTIP and PfMyoA (Douse *et al*., 2012). The corresponding serine residue in TgMLC1 (S113) was mutated however no change in the level of TgMyoA was observed in the co-IP. It is not possible to exclude that the two myosin light chains are differentially regulated by phosphorylation in the two organisms. Interestingly the phospho-peptides analysis performed in this study revealed two phosphorylation sites on TgMLC1 that were not described in the literature before S92 and S97. Since the analysis performed here cannot be claimed to be exhaustive, no strong conclusion can be drawn however, no cryptic phosphorylation site compensating for the mutations was identified in the MycMLC1-AAA. Given that not all the phosphorylation sites reported on MLC1 have been mutated here, we cannot exclude that this PTM impacts on the glideosome function.

In parallel, a similar mutagenesis approach was applied to TgGAP45 and the mutants were assessed for functional complementation in ΔGAP45e/MycGAP45i. Again the results revealed no significant impact of phosphorylation, except for the alanine substitution at residue T189 that resulted in a modest defect during calcium ionophore-induced egress. However, allelic replacement of the endogenous *TgGAP45* locus with this mutant showed no phenotype suggesting either a compensatory effect during the selection process or an adapted level of expression that allowed full complementation. During the generation of the different strains, we observed that the level of expression of the complemented copies critically contributed to the phenotype. Indeed, and logically, mutant copies expressed at low level failed to complement. Since none of the point mutations made in TgGAP45 had a phenotypic consequence for glideosome functions, the cluster of phosphorylation located in the DR was deleted entirely and the truncated TgGAP45 was assessed for functional complementation. Despite this substantial deletion, TyGAP45c-ΔDR was capable of fully replacing MycGAP45i. Mass spectrometry analyses revealed no additional compensatory

phosphorylation except in the N-terminal Ty tag. Given that the Ty tag is not part of the endogenous protein this phosphorylation is incidental and unlikely to have significant functional impact.

The interaction of the mutant S163/7E with IMC resident proteins TgGAP50 and TgGAP40 appeared to depend to some extent on the presence or absence of a wt copy of TgGAP45. It is possible that phosphorylation at residues S163/7 prevents a premature insertion of the glideosome within the IMC during daughter cell formation (Gilk *et al*., 2009). The pre-complex formed by TgGAP45/TgMyoA/TgMLC1 is first assembled in the cytoplasm and only recruited to the IMC in mature parasites (Gaskins *et al*., 2004; Frenal *et al*., 2010). The wt form of TgGAP45 apparently has a selective advantage to be inserted with the appropriate timing and hence competes with the mutant S163/7E. Additionally, the essential N-terminal acylation of TgGAP45 was also reported to prevent association of the pre-complex with the nascent IMC (Frenal *et al*., 2010). These findings suggest that different post-translational modifications contribute to the insertion of the motor at the pellicle in a temporally controlled manner; however, phosphorylation of the known modified sites is not absolutely required for this process. Concordantly, mutant S163/7A was not prematurely inserted in the IMC of nascent daughter cells.

In comparison to TgGAP45, PfGAP45 contains several additional phosphorylation sites in the coiled-coil region that were not reported to be modified on the *Toxoplasma* protein (Jacot and Soldati-Favre, 2012). Since PfGAP45 can functionally substitute for TgGAP45 (Frenal *et al*., 2010), these sites are either phosphorylated by *T. gondii* kinase(s) or not crucial. Supporting the second hypothesis, none of the episomally expressed phospho-mutants of PfGAP45 that have been analysed so far, revealed any significant impact on the assembly of the glideosome or PfGAP45 localization in blood stage malaria parasites (Ridzuan *et al*., 2012; Thomas *et al*., 2012).

How the glideosome is timely harnessed for concerted action during motility remains to be further investigated, however phosphorylation of the glideosome itself does not appear to play a central role. MyoA and GAP40 also contain phosphorylation sites that remain to be investigated and a cumulative effect of multiple phosphorylation events on one or more components of the glideosome cannot be excluded (at least 35 phosphorylation sites are associated with the glideosome) (Jacot and Soldati-Favre, 2012). This postulate is experimentally very complicated to address due to the vast number of possible combinations. It could also be conceivable that there is a large amount of noise in the phosphorylation process where numerous sites may have negligible consequences. Consistent with the results presented in this study, all the recent kinases implicated in egress affect microneme secretion (Lourido *et al*., 2010; 2012; Garrison *et al*., 2012; McCoy *et al*., 2012; Collins *et al*., 2013) and none so far have been attributed selectively to the glideosome function. Given the essential contribution of microneme proteins in egress, it was not possible to measure the impact on glideosome activation in situations where microneme secretion is simultaneously impaired.

Experimental procedures

T. gondii *culture*

T. gondii tachyzoites were grown in confluent human foreskin fibroblasts (HFFs) maintained in Dulbecco's modified Eagle's medium (DMEM; GIBCO, Invitrogen) supplemented with 10% fetal calf serum, 2 mM glutamine and 25 μg ml^{-1} gentamicin. Conditional expression was regulated with 0.5 μM Shld-1 for DD-fusion stabilization (Herm-Gotz *et al*., 2007) or with 1 μg ml^{-1} anhydrotetracycline (ATc) for the Tet-inducible system (Meissner *et al*., 2001).

Parasite transfection and selection of stable transgenic parasites

Parasite transfections were performed as previously reported (Soldati and Boothroyd, 1993). Selection of transgenic parasites was performed with both mycophenolic acid and xanthine for HXGPRT selection (Donald *et al*., 1996) and with phleomycin for bleomycin (BLE) selection (Messina *et al*., 1995). All strains were cloned by limiting dilution. The RH strain (Donald *et al*., 1996) was transfected with 60 μg of the following plasmids: pT8DDmyc-MLC1-mutants-HXGPRT (linearized with NotI). ΔKu80 (Huynh and Carruthers, 2009) was transfected with 40 μg of the following plasmids: MycMLC1cDNA-mutants-HXGPRT (linearized with EcoRV), GAP45Ty-HXGPRT (T189A, T189E, S163/7A, S163/7E and wt, linearized with BglII). ΔGAP45e/MycGAP45i (Frenal *et al*., 2010) was transfected with 60 μg of pT8-TyGAP45c-mutant-BLE and pT8-TyGAP45c-ΔDR-BLE (linearized with SacI). pT8, tubulin promoter.

Cloning of DNA constructs

Genomic DNA was isolated using the Wizard SV genomic DNA purification system (Promega). RNA was isolated using Trizol (Invitrogen) extraction. cDNA was generated by RT-PCR performed with Superscript II reverse transcriptase (Invitrogen) according to the manufacturer's protocol. Site directed mutagenesis was performed with the QuickChange II Site-Directed Mutagenesis Kit (200524, Agilent technologies) following the manufacturer's protocol. Primers used are presented in Table S1. Mutagenesis was performed in pGEM®-T Easy backbone and subcloned into the final vectors. All mutants were cloned following the same procedure. Mutants S239A and S239E were generated using reverse primers 4732 and 4733 respectively and forward primer 2258 with pT8-TyGAP45c-wt-BLE as template.

pT8DDmyc-TgMLC1-HXGPRT: TgMLC1 was amplified from RH cDNA using primers 2993-2995, digested with NsiI and PacI and cloned into pT8DDmycFH2-HX (Daher *et al*., 2010).

MycTgMLC1cDNA-HXGPRT: the homology fragment for recombination was amplified with primers 3458-3459, digested with KpnI and SbfI and cloned into pT8DDmyc-TgMLC1-HXGPRT. pT8-TyGAP45c-BLE: the Ty-tag was introduced by PCR by amplifying pT8 and NtGAP45 with primers T7-2786 with pT8MycGAP45 as template (Frenal *et al.*, 2010) and by subcloning this insert between KpnI and NsiI sites in the same vector. The BLE cassette was then amplified with primers 2787/2642, digested with SacII and cloned. pT8-TyGAP45c-ΔDR-BLE: NtGAP45Ty-CC and GAP45Ct were amplified with primers 2258–3961 and 3960–2383 respectively with TyGAP45 as template. GAP45Ct was digested with PstI and PacI and cloned into the same vector. NtGAP45Ty-CC was cloned into the PstI site of the resulting vector. GAP45Ty-HXGPRT: NtGAP45 was amplified from gDNA of ΔKu80 using primers 3993–3994 and primers 3995-3996. These two PCR products were first ligated to introduce a unique BglII site (between 3994–3995) and a Ty tag after 3996. This fragment was digested with KpnI and EcoRV and cloned into MycTgMLC1cDNA-HXGPRT. GAP45Ct was amplified using primers 3997–2383, digested with EcoRV and PacI, and cloned into the previous resulting vector. The corresponding pT8-TyGAP45c-BLE plasmids were used as templates for these PCRs.

All the primers used in this study are listed in Table S1.

Plaque assay

A confluent monolayer of HFFs was infected with freshly egressed parasites and treated ± ATc or ± Shld-1 for 7 days before the cells were fixed with paraformaldehyde/glutaraldehyde (PFA/GA). The host cell layer was then stained for 10 min at RT with Giemsa or crystal violet (Sigma-Aldrich). Data are representative of three independent biological experiments.

Egress assay

Freshly egressed parasites were allowed to invade HFF monolayers on coverslips and incubated for 2 h before washing of the host cells. A pre-treatment of 12 h (± ATc) was performed for parasites in the ΔGAP45e/MycGAP45i background. After 30 h of growth, parasites were treated for 7 min at 37°C with DMEM containing 0.06% DMSO or 3 μM calcium ionophore A23187 from *Streptomyces chartreusensis* (Calbiochem). Coverslips were fixed with PFA/GA and stained with anti-GAP45 antibodies. Two hundred vacuoles were counted for each strain and the number of egressed vacuoles is represented. Data are mean values ± SD from three independent biological experiments.

Intracellular growth assay

MycMLC1 parasites were grown for 30 h prior to fixation with PFA/GA. Immunofluorescence analyses using anti-GAP45 antibodies were performed and the number of parasites per vacuole was scored. Two hundred vacuoles were counted for each condition. Data are mean values ± SD from three independent biological experiments.

Competition assays

The different mutants were mixed with a parental strain at day 0 and the ratio of transgenic parasites was assessed by immunofluorescence analyses using anti-Ty or anti-Myc antibodies every 2 or 4 days. ΔKu80 was used as the parental strain for the GAP45Ty and MycMLC1 strains and RH was used for the TyGAP45c and ΔGAP45e/MycGAP45i strains. Regulation of MycGAP45i by ATc was assessed at days 6 and 16.

Antibodies

The antibodies used in this study are as follows: rabbit polyclonal; α-CAT (Ding *et al.*, 2000), α-GAP45 (Plattner *et al.*, 2008), α-MLC1 (Herm-Gotz *et al.*, 2002), α-GAP40, α-GAP50 (Jones *et al.*, 2009); mouse monoclonal, α-ACT (Herm-Gotz *et al.*, 2002), α-Ty (BB2), α-Myc (9E10). For Western blot analyses, secondary peroxidase-conjugated goat α-rabbit/mouse antibodies (Molecular Probes) were used as well as Alexa Fluor 694-conjugated goat α-mouse/rabbit antibodies. For immunofluorescence analyses, the secondary antibodies Alexa Fluor 488 and Alexa Fluor 594-conjugated goat α-mouse/rabbit antibodies (Molecular Probes) were used.

To generate the anti-GAP40 antibodies, two peptides (H2N-GGENYADVCDDEAHSS-COOH and AcNH-KNIVSNRLIRRTGQAP-CONH2) were synthesized and used to immunize two rabbits according to the Eurogentec standard protocol.

Metabolic labelling and co-immunoprecipitation

Freshly egressed parasites were harvested and incubated for 15 min in methionine/cysteine-free DMEM (Sigma). Parasites were harvested and re-suspended in DMEM containing 10 μCi [35S]-labelled methionine/cysteine (Hartmann analytic GmbH) per ml for 4 h. Parasites were lysed in CoIP buffer [1% (v/v) Triton X-100, 50 mM Tris-HCl, pH 8, 150 mM NaCl] in the presence of a protease inhibitor cocktail (Roche). Cells were incubated for 10 min on ice, frozen and thawed, sonicated and centrifuged at 14 000 rpm for 30 min. Supernatants were incubated with corresponding antibodies as previously described (Gaskins *et al.*, 2004). All samples were boiled prior to SDS-PAGE.

DDMycMLC1 were treated with Shld-1 24 h prior to the co-IP. TyGAP45c was treated ± ATc for 48 h.

Immunofluorescence assay and confocal microscopy

HFFs seeded on coverslips in 24-well plates were inoculated with freshly released parasites. After 2–5 rounds of parasite replication, cells were fixed with 4% paraformaldehyde (PFA) or 4% PFA/0.05% glutaraldehyde (PFA/GA) in PBS, neutralized 3–5 min in 0.1 M glycine/PBS, and processed as previously described (Plattner *et al.*, 2008). Confocal images were generated with a Zeiss laser scanning confocal microscope (LSM700, objective apochromat 63×/1.4 oil) at the bioimaging facility of the Faculty of Medicine, University of Geneva.

Western blot analyses

Parasites were lysed in RIPA buffer (150 mM NaCl, 1% Triton X-100, 0.5% deoxycholate, 0.1% SDS, 50 mM Tris pH 7.5) using standard procedures and mixed with SDS-PAGE loading buffer under reducing conditions. Suspension was subjected to two

sonication cycles. SDS-PAGE was performed using standard methods. Separated proteins were transferred to nitrocellulose membranes and probed with appropriate antibodies in 5% non-fat milk powder in 1× PBS-0.05% Tween 20. Bound secondary peroxidase conjugated antibodies were visualized using either the ECL system (GE healthcare) or SuperSignal (Pierce).

Mass spectrometry (MS)

In gel digestion. Gel fragments obtained after one-dimensional electrophoresis (1-DE) were first destained by incubation in 50 mM ammonium bicarbonate and 30% acetonitrile (AcN) for 30 min at room temperature. Destaining solution was removed and fragments were then incubated for 35 min at 56°C in 10 mM DTT in 50 mM ammonium bicarbonate. DTT solution was then replaced by 55 mM iodoacetamide in 50 mM ammonium bicarbonate and the gel fragments were incubated for 30 min at room temperature in the dark. Gel pieces were then washed for 30 min with 50 mM ammonium bicarbonate and for 30 min with 50 mM ammonium bicarbonate and 30% AcN. Gel pieces were then dried for 45 min in a Centrivap vacuum centrifuge (Labconco, Kansas City, USA). Dried pieces of gel were rehydrated for 45 min at 4°C in 50 mM ammonium bicarbonate containing trypsin at 6.25 ng μl^{-1}. Extraction of the peptides was performed with 1% TFA for 30 min at room temperature with occasional shaking. The TFA solution containing the proteins was transferred to a polypropylene tube. A second extraction of the peptides was performed with 0.1% TFA in 50% AcN for 30 min at room temperature with occasional shaking. The second TFA solution was pooled with the first one. The volume of the pooled extracts was completely dried by evaporation under vacuum.

Phosphopeptides enrichment. Performed following Larsen protocol (Jensen and Larsen, 2007). Briefly: stage-tips were home-made prepared using a small plug made of Glass Microfibre Filters (Whatman), and 5 μm TiO_2 beads (GL SCIENCES) to make a 5-mm-long column. TiO_2 beads were suspended in 0.1% TFA in 80% acetonitrile. Peptides were loaded onto TiO_2 column in 1 M glycolic acid 2% TFA in 80% acetonitrile then column was washed four times with 1 M glycolic acid 2% TFA in 80% acetonitrile and four times 0.1% TFA in 80% acetonitrile. Bounded peptides were eluted with 3% NH_4OH and 0.1% TFA in 80% acetonitrile then acidified with 5% TFA. Peptides were dried and resuspended in 16 μ of 5% ACN, 0.1% FA for MS analysis.

MS analysis. LC-ESI-MS/MS was performed on a linear trap quadrupole (LTQ) Orbitrap Velos (Thermo Electron, San Jose, CA, USA) equipped with a NanoAcquity system (Waters). Peptides were trapped on a home-made 5 μm 200 Å Magic C18 AQ (Michrom) 0.1 × 20 mm pre-column and separated on a commercial 0.075 × 150 mm Nikkyo (Nikkyo Technology) analytical nanocolumn (C18, 5 μm, 100 Å). The analytical separation was run for 17 min using a gradient of H_2O/FA 99.9%/0.1% (solvent A) and CH_3CN/FA 99.9%/0.1% (solvent B). The gradient was run as follows: 0–1 min 95% A and 5% B, then to 65% A and 35% B for 15 min, and 20% A and 80% B for 17 min at a flow rate of 220 nl min^{-1}. For MS survey scans, the orbitrap (OT) resolution was set to 60000 and the ion population was set to 5×10^5 with an m/z window from 400 to 2000. For protein identification, up to 5 precursor ions were selected for collision-induced dissociation (CID) in the LTQ. Multistage activation (MSA) of frequencies corresponding to neutral loss of phosphoric acid (–98, –49 and –32.6 Th relative to the precursor ion) was performed. The ion population was set to 1×10^4 (isolation width of 2 m/z). The normalized collision energies were set to 35% for CID.

Protein identification. Peak lists (MGF file format) were generated from raw orbitrap data using the EasyProtConv conversion tool from the EasyProt software platform (Gluck *et al.*, 2013). The peaklist files were searched against the *Toxoplasma gondii* GT1 database (Toxoplasma Genomics Resource, release 10.0 of 31-Jan-2014, 8461 entries, 6648588 residues) using Mascot (Matrix Sciences, London, UK). Sequences of modified GAP45 and MLC1 (tagged WT and mutants) proteins were inserted in *Toxoplasma* database. The parent ion tolerance was set to 10 ppm. Variable amino acid modifications were oxidized methionine and phosphorylated serine, threonine and tyrosine. Fixed amino acid modification was carbamidomethyl cystein. Trypsin was selected as the enzyme, with one potential missed cleavage, and the normal cleavage mode was used. The mascot search was validated using Scaffold 4.0.4 (Proteome Software, Portland, OR). Only proteins matching with two different peptides with a minimum probability score of 95% were considered identified.

Raw data of the TiO2 enriched fractions are presented in Table S2 for MLC1 and GAP45.

Acknowledgements

We are grateful to Dr Chris Tonkin for providing us with information of the mapping of TgMLC1 phosphorylation sites prior to publication. We thank Dr Julian Rayner for kindly providing anti-GAP50 antibodies. We thank Dr Manuel Gonzalez and Dr Arnault Graindorge for technical assistance and Dr Hayley Bullen for critical reading of the manuscript. D.J. was supported by the Indo-Swiss Joint Research Programme. P.S. is a recipient of the Swarnajayanti fellowship from the Department of Science and Technology, India. D.S.F. is an international advanced scholar of the HHMI. The research leading to these results has received funding from the European Union Seventh Framework Programme (FP7/2007-2013) under grant agreement no. 242095-EVIMalaR and the Swiss National Foundation (FN3100A0-116722).

Conflict of interest

The authors declare to have no conflict of interest.

References

Andenmatten, N., Egarter, S., Jackson, A.J., Jullien, N., Herman, J.P., and Meissner, M. (2013) Conditional genome engineering in *Toxoplasma gondii* uncovers alternative invasion mechanisms. *Nat Methods* **10:** 125–127.

Aurrecoechea, C., Heiges, M., Wang, H., Wang, Z., Fischer, S., Rhodes, P., *et al.* (2007) ApiDB: integrated resources for the apicomplexan bioinformatics resource center. *Nucleic Acids Res* **35:** D427–D430.

Azevedo, M.F., Sanders, P.R., Krejany, E., Nie, C.Q., Fu, P., Bach, L.A., *et al.* (2013) Inhibition of *Plasmodium falciparum* CDPK1 by conditional expression of its

J-domain demonstrates a key role in schizont development. *Biochem J* **452:** 433–441.

Billker, O., Lourido, S., and Sibley, L.D. (2009) Calcium-dependent signaling and kinases in apicomplexan parasites. *Cell Host Microbe* **5:** 612–622.

Carruthers, V., and Boothroyd, J.C. (2007) Pulling together: an integrated model of *Toxoplasma* cell invasion. *Curr Opin Microbiol* **10:** 83–89.

Carruthers, V.B., and Sibley, L.D. (1999) Mobilization of intracellular calcium stimulates microneme discharge in *Toxoplasma gondii*. *Mol Microbiol* **31:** 421–428.

Collins, C.R., Hackett, F., Strath, M., Penzo, M., Withers-Martinez, C., Baker, D.A., and Blackman, M.J. (2013) Malaria parasite cGMP-dependent protein kinase regulates blood stage merozoite secretory organelle discharge and egress. *PLoS Pathog* **9:** e1003344.

Daher, W., Plattner, F., Carlier, M.F., and Soldati-Favre, D. (2010) Concerted action of two formins in gliding motility and host cell invasion by *Toxoplasma gondii*. *PLoS Pathog* **6:** e1001132.

Delbac, F., Sanger, A., Neuhaus, E.M., Stratmann, R., Ajioka, J.W., Toursel, C., *et al*. (2001) *Toxoplasma gondii* myosins B/C: one gene, two tails, two localizations, and a role in parasite division. *J Cell Biol* **155:** 613–623.

Ding, M., Clayton, C., and Soldati, D. (2000) *Toxoplasma gondii* catalase: are there peroxisomes in toxoplasma? *J Cell Sci* **113:** 2409–2419.

Dobrowolski, J.M., and Sibley, L.D. (1996) *Toxoplasma* invasion of mammalian cells is powered by the actin cytoskeleton of the parasite. *Cell* **84:** 933–939.

Donald, R.G., Carter, D., Ullman, B., and Roos, D.S. (1996) Insertional tagging, cloning, and expression of the *Toxoplasma gondii* hypoxanthine-xanthine-guanine phosphoribosyltransferase gene. Use as a selectable marker for stable transformation. *J Biol Chem* **271:** 14010–14019.

Douse, C.H., Green, J.L., Salgado, P.S., Simpson, P.J., Thomas, J.C., Langsley, G., *et al*. (2012) Regulation of the *Plasmodium* motor complex: phosphorylation of myosin A tail-interacting protein (MTIP) loosens its grip on MyoA. *J Biol Chem* **287:** 36968–36977.

Frenal, K., Polonais, V., Marq, J.B., Stratmann, R., Limenitakis, J., and Soldati-Favre, D. (2010) Functional dissection of the apicomplexan glideosome molecular architecture. *Cell Host Microbe* **8:** 343–357.

Garrison, E., Treeck, M., Ehret, E., Butz, H., Garbuz, T., Oswald, B.P., *et al*. (2012) A forward genetic screen reveals that calcium-dependent protein kinase 3 regulates egress in *Toxoplasma*. *PLoS Pathog* **8:** e1003049.

Gaskins, E., Gilk, S., DeVore, N., Mann, T., Ward, G., and Beckers, C. (2004) Identification of the membrane receptor of a class XIV myosin in *Toxoplasma gondii*. *J Cell Biol* **165:** 383–393.

Gilk, S.D., Gaskins, E., Ward, G.E., and Beckers, C.J. (2009) GAP45 phosphorylation controls assembly of the *Toxoplasma* myosin XIV complex. *Eukaryot Cell* **8:** 190–196.

Gluck, F., Hoogland, C., Antinori, P., Robin, X., Nikitin, F., Zufferey, A., *et al*. (2013) EasyProt – an easy-to-use graphical platform for proteomics data analysis. *J Proteomics* **79:** 146–160.

Gouy, M., Guindon, S., and Gascuel, O. (2010) SeaView version 4: a multiplatform graphical user interface for sequence alignment and phylogenetic tree building. *Mol Biol Evol* **27:** 221–224.

Green, J.L., Rees-Channer, R.R., Howell, S.A., Martin, S.R., Knuepfer, E., Taylor, H.M., *et al*. (2008) The motor complex of *Plasmodium falciparum*: phosphorylation by a calcium-dependent protein kinase. *J Biol Chem* **283:** 30980–30989.

Herm-Gotz, A., Weiss, S., Stratmann, R., Fujita-Becker, S., Ruff, C., Meyhofer, E., *et al*. (2002) *Toxoplasma gondii* myosin A and its light chain: a fast, single-headed, plus-end-directed motor. *EMBO J* **21:** 2149–2158.

Herm-Gotz, A., Agop-Nersesian, C., Munter, S., Grimley, J.S., Wandless, T.J., Frischknecht, F., and Meissner, M. (2007) Rapid control of protein level in the apicomplexan *Toxoplasma gondii*. *Nat Methods* **4:** 1003–1005.

Huynh, M.H., and Carruthers, V.B. (2009) Tagging of endogenous genes in a *Toxoplasma gondii* strain lacking Ku80. *Eukaryot Cell* **8:** 530–539.

Jacot, D., and Soldati-Favre, D. (2012) Does protein phosphorylation govern host cell entry and egress by the Apicomplexa? *Int J Med Microbiol* **302:** 195–202.

Jensen, S.S., and Larsen, M.R. (2007) Evaluation of the impact of some experimental procedures on different phosphopeptide enrichment techniques. *Rapid Commun Mass Spectrom* **21:** 3635–3645.

Jones, M.L., Cottingham, C., and Rayner, J.C. (2009) Effects of calcium signaling on *Plasmodium falciparum* erythrocyte invasion and post-translational modification of gliding-associated protein 45 (PfGAP45). *Mol Biochem Parasitol* **168:** 55–62.

Kato, N., Sakata, T., Breton, G., Le Roch, K.G., Nagle, A., Andersen, C., *et al*. (2008) Gene expression signatures and small-molecule compounds link a protein kinase to *Plasmodium falciparum* motility. *Nat Chem Biol* **4:** 347–356.

Keeley, A., and Soldati, D. (2004) The glideosome: a molecular machine powering motility and host-cell invasion by Apicomplexa. *Trends Cell Biol* **14:** 528–532.

Lasonder, E., Green, J.L., Camarda, G., Talabani, H., Holder, A.A., Langsley, G., and Alano, P. (2012) The *Plasmodium falciparum* schizont phosphoproteome reveals extensive phosphatidylinositol and cAMP-protein kinase A signaling. *J Proteome Res* **11:** 5323–5337.

Lourido, S., Shuman, J., Zhang, C., Shokat, K.M., Hui, R., and Sibley, L.D. (2010) Calcium-dependent protein kinase 1 is an essential regulator of exocytosis in *Toxoplasma*. *Nature* **465:** 359–362.

Lourido, S., Tang, K., and Sibley, L.D. (2012) Distinct signalling pathways control Toxoplasma egress and host-cell invasion. *EMBO J* **31:** 4524–4534.

Lovett, J.L., and Sibley, L.D. (2003) Intracellular calcium stores in *Toxoplasma gondii* govern invasion of host cells. *J Cell Sci* **116:** 3009–3016.

McCoy, J.M., Whitehead, L., van Dooren, G.G., and Tonkin, C.J. (2012) TgCDPK3 regulates calcium-dependent egress of *Toxoplasma gondii* from host cells. *PLoS Pathog* **8:** e1003066.

Meissner, M., Brecht, S., Bujard, H., and Soldati, D. (2001) Modulation of myosin A expression by a newly established tetracycline repressor-based inducible system in *Toxoplasma gondii*. *Nucleic Acids Res* **29:** E115.

Meissner, M., Schluter, D., and Soldati, D. (2002) Role of *Toxoplasma gondii* myosin A in powering parasite gliding and host cell invasion. *Science* **298:** 837–840.

Messina, M., Niesman, I., Mercier, C., and Sibley, L.D. (1995) Stable DNA transformation of *Toxoplasma gondii* using phleomycin selection. *Gene* **165:** 213–217.

Montoya, J.G., and Liesenfeld, O. (2004) Toxoplasmosis. *Lancet* **363:** 1965–1976.

Morrissette, N.S., and Sibley, L.D. (2002) Cytoskeleton of apicomplexan parasites. *Microbiol Mol Biol Rev* **66:** 21–38.

Murray, C.J., Rosenfeld, L.C., Lim, S.S., Andrews, K.G., Foreman, K.J., Haring, D., *et al*. (2012) Global malaria mortality between 1980 and 2010: a systematic analysis. *Lancet* **379:** 413–431.

Nebl, T., Prieto, J.H., Kapp, E., Smith, B.J., Williams, M.J., Yates, J.R., 3rd, *et al*. (2011) Quantitative in vivo analyses reveal calcium-dependent phosphorylation sites and identifies a novel component of the *Toxoplasma* invasion motor complex. *PLoS Pathog* **7:** e1002222.

Opitz, C., and Soldati, D. (2002) The glideosome': a dynamic complex powering gliding motion and host cell invasion by *Toxoplasma gondii*. *Mol Microbiol* **45:** 597–604.

Pease, B.N., Huttlin, E.L., Jedrychowski, M.P., Talevich, E., Harmon, J., Dillman, T., *et al*. (2013) Global Analysis of Protein Expression and Phosphorylation of Three Stages of *Plasmodium falciparum* Intraerythrocytic Development. *J Proteome Res* **12:** 4028–4045.

Plattner, F., Yarovinsky, F., Romero, S., Didry, D., Carlier, M.F., Sher, A., and Soldati-Favre, D. (2008) *Toxoplasma* profilin is essential for host cell invasion and TLR11-dependent induction of an interleukin-12 response. *Cell Host Microbe* **3:** 77–87.

Polonais, V., Javier Foth, B., Chinthalapudi, K., Marq, J.B., Manstein, D.J., Soldati-Favre, D., and Frenal, K. (2011) Unusual anchor of a motor complex (MyoD-MLC2) to the plasma membrane of *Toxoplasma gondii*. *Traffic* **12:** 287–300.

Rees-Channer, R.R., Martin, S.R., Green, J.L., Bowyer, P.W., Grainger, M., Molloy, J.E., and Holder, A.A. (2006) Dual acylation of the 45 kDa gliding-associated protein (GAP45) in *Plasmodium falciparum* merozoites. *Mol Biochem Parasitol* **149:** 113–116.

Ridzuan, M.A., Moon, R.W., Knuepfer, E., Black, S., Holder, A.A., and Green, J.L. (2012) Subcellular location, phosphorylation and assembly into the motor complex of GAP45 during *Plasmodium falciparum* schizont development. *PLoS ONE* **7:** e33845.

Soldati, D., and Boothroyd, J.C. (1993) Transient transfection and expression in the obligate intracellular parasite *Toxoplasma gondii*. *Science* **260:** 349–352.

Solyakov, L., Halbert, J., Alam, M.M., Semblat, J.P., Dorin-Semblat, D., Reininger, L., *et al*. (2011) Global kinomic and phospho-proteomic analyses of the human malaria parasite *Plasmodium falciparum*. *Nat Commun* **2:** 565.

Tewari, R., Straschil, U., Bateman, A., Bohme, U., Cherevach, I., Gong, P., *et al*. (2010) The systematic functional analysis of *Plasmodium* protein kinases identifies essential regulators of mosquito transmission. *Cell Host Microbe* **8:** 377–387.

Thomas, D.C., Ahmed, A., Gilberger, T.W., and Sharma, P. (2012) Regulation of *Plasmodium falciparum* glideosome associated protein 45 (PfGAP45) phosphorylation. *PLoS ONE* **7:** e35855.

Treeck, M., Sanders, J.L., Elias, J.E., and Boothroyd, J.C. (2011) The phosphoproteomes of *Plasmodium falciparum* and *Toxoplasma gondii* reveal unusual adaptations within and beyond the parasites' boundaries. *Cell Host Microbe* **10:** 410–419.

Tyler, J.S., Treeck, M., and Boothroyd, J.C. (2011) Focus on the ringleader: the role of AMA1 in apicomplexan invasion and replication. *Trends Parasitol* **27:** 410–420.

Vaid, A., Thomas, D.C., and Sharma, P. (2008) Role of Ca2+/calmodulin-PfPKB signaling pathway in erythrocyte invasion by *Plasmodium falciparum*. *J Biol Chem* **283:** 5589–5597.

Wetzel, D.M., Hakansson, S., Hu, K., Roos, D., and Sibley, L.D. (2003) Actin filament polymerization regulates gliding motility by apicomplexan parasites. *Mol Biol Cell* **14:** 396–406.

Winter, D., Kugelstadt, D., Seidler, J., Kappes, B., and Lehmann, W.D. (2009) Protein phosphorylation influences proteolytic cleavage and kinase substrate properties exemplified by analysis of *in vitro* phosphorylated *Plasmodium falciparum* glideosome-associated protein 45 by nano-ultra performance liquid chromatography-tandem mass spectrometry. *Anal Biochem* **393:** 41–47.

Supporting information

Additional Supporting Information may be found in the online version of this article at the publisher's web-site:

Fig. S1. A. Multiple alignment of apicomplexan myosin light chain 1 (Myosin A interacting protein, MTIP in *Plasmodium*) performed with seaview, alignment algorithm muscle (Gouy *et al*., 2010). Red, phosphorylation sites investigated in this study; pink, phosphorylation sites found *in vivo*. Accession numbers from eupathDB (Aurrecoechea *et al*., 2007): *Toxoplasma gondii* (Tg), TGME49_257680; *Neospora caninum* (Nc), NCLIV_029420; *Plasmodium falciparum* (Pf), PF3D7_1246400; *Theileria annulata* (Ta), TA20485; *Babesia bovis* (Bb), BBOV_III002630.

B. Immunofluorescence analyses using anti-Myc antibodies of DDMycMLC1 constructs showed proper localization to the pellicle in the presence of Shld-1 for 24 h. Scale bar 2 μm.

C. The different DDMycMLC1 expressing strains formed plaques of similar sizes ± Shld-1.

D. Schematic representation of the knock-in strategy for TgMLC1 (not to scale). We took advantage of the unusual topology of the locus with a first non-coding exon and a large first intron to insert, by single homologous recombination, mutated forms of TgMLC1 which results in the displacement of the endogenous TgMLC1. Grey, mRNA; green, homology region for recombination.

E. PCR analyses of the recombinant locus of MycMLC1 strains using primers A/B found in table S1 and depicted in panel D. No amplification was detected in the parental ΔKu80 strain.

F. The different MycMLC1 strains showed no defect in intracellular growth after 30 h compared with ΔKu80.

Fig. S2. Multiple alignment of apicomplexan TgGAP45 performed with seaview, alignment algorithm muscle (Gouy *et al*., 2010). Red, phosphorylation sites investigated in this study; pink, phosphorylation sites found *in vivo*. Accession numbers from

eupathDB (Aurrecoechea *et al*., 2007): *Toxoplasma gondii* (Tg), TGME49_223940; *Neospora caninum* (Nc), NCLIV_048570; *Plasmodium falciparum* (Pf), PF3D7_1222700; *Theileria annulata* (Ta), TA13510; *Babesia bovis* (Bb), BBOV_II005470.

Fig. S3. (A) Schematic representation of TgMLC1 highlighting the previously reported phosphorylation sites (Treeck *et al*., 2011). The sites investigated in this study are in red. Schematic representation of MycMLC1-wt (B) and MycMLC1-AAA (C) phosphorylation sites identified by mass spectrometry in this study and presentation of the corresponding spectra. The Myc tag was not included in the amino acid numbering.

Fig. S4. (A) Schematic representation of TgGAP45 highlighting the previously reported phosphorylation sites (Nebl *et al*., 2011; Treeck *et al*., 2011). In red are the sites investigated in this study. Schematic representation of TyGAP45c-wt (B) and TyGAP45c-ΔDR (C) phosphorylation sites identified by mass spectrometry in this study and presentation of the related most relevant spectra. Phosphorylation in the Ty tag is highlighted in red. The Ty tag was not included in the amino acid numbering.

Table S1. Primers used in this study.

Table S2. Raw data of the TiO2 enriched fractions for identification of the phosphorylation sites of MLC1 and GAP45.